ACS APPLIED MATERIALS & INTERFACES

www.acsami.org

Research Article

Self-Assembled DNA Nanoflowers Triggered by a DNA Walker for Highly Sensitive Electrochemical Detection of *Staphylococcus aureus*

Rongfeng Cai, Shixin Zhang, Luo Chen, Maolin Li,* Yuting Zhang, and Nandi Zhou*

Cite This: *ACS Appl. Mater. Interfaces* 2021, 13, 4905–4914

Read Online

ACCESS | Metrics & More | Article Recommendations | Supporting Information

ABSTRACT: With the development of DNA nanotechnology, DNA has been widely used to construct a variety of nanomachines. Among them, a DNA walker is a unique nanomachine that can move continuously along a specific orbit to fulfill diverse functions. In this paper, a dual signal amplification electrochemical biosensor based on a DNA walker and DNA nanoflowers is constructed for high sensitivity detection of *Staphylococcus aureus* (*S. aureus*). Two groups of double-stranded DNA are modified on the surface of a gold electrode. The binding of *S. aureus* with its aptamer induces the disintegration of the long double strands and releases the DNA walker. With the help of exonuclease III (Exo III), the DNA walker moves along the electrode surface and continuously hydrolyzes the anchored short double strands. The introduction of a specially customized circular DNA and phi29 DNA polymerase initiates the rolling circle amplification (RCA) reaction. DNA nanoflowers are formed at high local concentration of DNA in the solution, which provide binding sites for electroactive methylene blue (MB) and thus produce intense signal. Under the best conditions, the current response is linearly related to the logarithm of the concentration of *S. aureus* ranging from 60 to 6 × 10^7 CFU/mL, and the detection limit is 9 CFU/mL. In addition, the proposed biosensor has achieved satisfactory results in the detection of actual water samples and diluted honey samples, which confirm the practicability of the biosensor and its application potential in environmental monitoring and food safety.

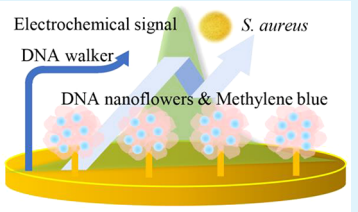

KEYWORDS: *Staphylococcus aureus, DNA walker, rolling circle amplification, DNA nanoflowers, electrochemical biosensor*

1. INTRODUCTION

DNA is the main carrier of organism genetic information, and its replication process follows the strict base-pairing principle to ensure the accuracy of genetic information transmission. Owing to such a property, DNA has also been used as a scaffold to achieve the synthesis of DNA nanomaterials with low nanometer precision.[1,2] A variety of DNA nanostructures have been designed and constructed, which makes DNA nanotechnology infiltrate into biomedical,[3] chemical,[4] materials,[5] and other fields. For example, a DNA tetrahedron,[6] DNA nanomaterial with 3D structure, can penetrate the cell membranes without transfection agents for intracellular detection or cargo transport,[7] which provides an alternative method for molecular diagnosis[8] and new drug development.[9] Compared with traditional nanomaterials,[10,11] DNA nanomaterials have good biocompatibility and broad application prospects in biomedicine and biotechnology.[12]

In addition to the construction of static DNA nanomaterials, DNA can also be used to form molecular machines with dynamic behaviors.[13] Similar to the motor proteins responsible for the movement of part of the cell or the whole cell, a DNA walker is a kind of nanoscale molecular device driven by environmental stimulation, enzyme reaction, or strand displacement reaction.[14,15] It can carry out repeated mechanical cycle movement along the DNA orbit composed of part or all of nucleic acids to realize signal cascade amplification.[16] Signal amplification methods based on DNA walkers have attracted wide attention because of their simple structures, easy synthesis, sequence predictability, and programmability.[17] Combined with biosensors, the changes of DNA components can be triggered by specific target binding.[18] Then the repeated DNA hybridization can be performed by enzyme-mediated DNA substrate hydrolysis or toehold-mediated strand displacement.[19] Finally, the target binding-induced DNA walker can activate hundreds of signal molecules to respond to a single highly specific binding, which provides a promising tool for designing signal amplification methods.[20]

Different from the traditional preparation methods of DNA nanomaterials, the synthesis of some DNA nanomaterials does not depend entirely on the principle of base complementary pairing.[21] For example, DNA nanoflowers can be synthesized by liquid crystallization and self-assembly of local high concentration of DNA.[22] Under the mild reaction conditions, two DNA strands and phi29 DNA polymerase can generate DNA nanoflowers with the diameters ranging from tens to hundreds of nanometers.[23] Studies have shown that DNA nanoflowers have good stability and can effectively resist the

Received: December 13, 2020
Accepted: January 14, 2021
Published: January 20, 2021

https://dx.doi.org/10.1021/acsami.0c22062
ACS Appl. Mater. Interfaces 2021, 13, 4905–4914

attack of exonuclease,[24] so they are often used as drug carriers and are responsible for the targeted transport of drugs in organisms.[25] Because DNA nanoflowers can be synthesized with only a small amount of DNA and enzyme triggers, they can be designed as ideal signal amplifiers. However, few studies so far exert the properties of DNA nanoflowers in this area.[26]

The combination of DNA nanotechnology and biosensors can develop new types of biosensors with effectively improved performance.[27] The chemical and physical properties of DNA nanomaterials, such as small size effect and surface effect, are exactly corresponding to the miniaturization and multifunction required by biosensors.[27] Commonly used components in biosensor construction include enzymes,[28] antibodies,[29] nucleic acids, and so on. Among them, aptamer is a kind of oligonucleotide with high affinity and specificity to targets, also known as "chemical antibodies".[30] Compared with antibodies, aptamers have the advantages of a short SELEX process, small differences between production batches, and easy preservation and transportation and are often used in the construction of various biosensors, targeted drug transport, intracellular imaging, and other fields. Particularly, the nucleic acid nature of aptamers makes them easy to integrate into DNA nanostructures. Aptamers combine electrodes, photoelectric converters, thermistors, piezoelectric crystals. and other devices to convert biological information into electrical,[31] optical,[32] temperature,[33] and other signal outputs, providing a wealth of means for the detection of a biochemical reaction process.

Staphylococcus aureus (*S. aureus*) is a food-borne pathogen that widely exists in the environment. The enterotoxin produced by *S. aureus* can cause food poisoning and various infections.[34] Therefore, constructing accurate and sensitive detection methods for *S. aureus* has become an urgent topic. At present, a variety of *S. aureus* aptasensors have been reported, such as colorimetric biosensors,[35] optical biosensors,[36] and electrochemical biosensors.[37] Electrochemical biosensors have attracted wide attention because of their high sensitivity.[38] Inspired by the above strategies, an electrochemical biosensor based on a DNA walker and DNA nanoflowers has been developed for the determination of *S. aureus*. Taking advantage of the high affinity and specificity of the aptamer, the mechanical movement of the molecular machines, and the unique property of the DNA nanoflowers, a highly sensitive determination of *S. aureus* has been realized. In this platform, a DNA walker is introduced to move periodically on the electrode surface to ensure the releasing of a large number of primers used for rolling circle amplification (RCA) reaction and realize signal amplification. The formation of DNA nanoflowers increases the effective area of the electrode surface, and the combination of a large number of electroactive methylene blue (MB) improves the electron transfer efficiency of the electrode. The platform has good sensitivity, specificity, and stability, which shows great potential in food safety and environmental monitoring.

2. EXPERIMENTAL SECTION

2.1. Materials and Regents. Exo III and T4 DNA ligase were purchased from New England Biolabs Ltd. (Beijing, China). 6-Mercaptohexanol (6-MCH) was obtained from Sigma-Aldrich Ltd. (Shanghai, China). GelRed nucleic acid gel stain was purchased from Biotium Inc. (Fremont, CA). Phi29 DNA polymerase was obtained from CoWin Biosciences Ltd. (Beijing, China). MB was purchased from Sinopharm Chemical Reagent Co., Ltd. (Shanghai, China). All other chemicals in the experiment are analytical reagents and can be used without further purification. Throughout the experiment, ultrapure water with a resistivity of 18.2 MΩ cm obtained from the microporous filtration system (Billerica, MA) was used to prepare the solution.

The *S. aureus* aptamer,[39] rolling circle amplification reaction primer (RP), walker sequence (W), auxiliary sequence (AS), and circular template sequence (CT) were optimized and are shown in Table S1 of the Supporting Information. All sequences used in this paper were synthesized, modified, and purified by Sangon Biotech Co., Ltd. (Shanghai, China).

2.2. Bacterial Strains, Cultivation, and Preparation. The strains *S. aureus* ATCC 29213, *Enterococcus faecium* (*E. faecium* ATCC 19434), *Listeria monocytogenes* (*L. monocytogenes* BNCC 336877), *Pseudomonas aeruginosa* (*P. aeruginosa*), *Enterococcus faecalis* (*E. faecalis* ATCC 19433), and *Salmonella enteritidis* (*S. enteritidis* BNCC103134) were preserved in our laboratory.

S. aureus preserved at −40 °C was activated by plate marking, then inoculated into the LB medium, and cultured at 37 °C at 220 rpm until logarithmic growth phase. The bacterial solution was centrifuged at 3000 rpm for 5 min to remove the culture medium in the supernatant. The collected bacterial precipitate was washed gently with 10 mM PBS buffer (containing 100 mM KCl, pH 7.0) to remove the remaining medium. After washing for three times, the bacterial precipitate was dissolved in PBS buffer and stored at 4 °C. To calculate the exact number of bacteria in LB medium, the bacterial suspension was continuously diluted with PBS buffer at a gradient of 10 times. A 100 μL aliquot of diluted bacteria solution was incubated on an LB plate at 37 °C for 24 h, and the colony number on the plate was determined and expressed as CFU/mL. Other bacteria used for the specificity study of the sensor were cultured under the same conditions.

2.3. Preparation and Modification of Gold Electrode. First, 30% H_2O_2 and H_2SO_4 were used to prepare a piranha solution according to the formula of H_2O_2:H_2SO_4 = 3:7. The gold electrode was immersed in the piranha solution for 15 min to remove impurities on the surface. The electrode surface was then washed and transferred to ultrapure water for ultrasonication for 5 min. The surface of the electrode was electrochemically cleaned with 0.5 M H_2SO_4 to activate the electrode. Finally, the electrode was washed with ultrapure water again and gently dried with nitrogen to keep the electrode surface smooth and clean.

To prepare the solution used to modify the gold electrode, 2 μL of 1 μM W and 4 μL of 1 μM aptamer were added to 4 μL of PBS buffer. We added 1 μL of 10 μM RP and 2 μL of 10 μM AS to 7 μL of PBS buffer. Then the mixtures were thermally denatured at 95 °C for 10 min and then placed in a 4 °C ice bath for 10 min to form aptamer/W and AS/RP duplexes, respectively.

Subsequently, the aptamer/W duplex and AS/RP duplex were mixed evenly. Then a 10 μL mixture was dropped on the cleaned electrode surface and incubated at 30 °C for 12 h, so that the two groups of double-stranded structures can be modified onto the surface of the electrode via the Au−S bond. The modified gold electrode was washed with ultrapure water for 15 s to remove the excess DNA due to physical adsorption. After two groups of double-stranded structures were captured on the gold electrode, the electrode was immediately placed in 100 μL of a 1 M 6-MCH solution at room temperature for 60 min to avoid the nonspecific adsorption of other DNA on the electrode surface.

2.4. *S. aureus* Detection Procedure. PBS buffer (100 μL) containing different concentrations of *S. aureus* was spread evenly on the modified electrode. After incubation at 37 °C for 60 min, the electrode was gently washed with PBS buffer. To realize the walking and cutting function of DNA walker on the electrode surface, 10 μL of Exo III digestion solution consisting of 0.75 μL of 10 U/μL Exo III, 1 μL 10 × Exo III reaction buffer, and 8.25 μL ddH_2O was spread on the electrode and kept at 37 °C for 80 min. After digestion reaction, the electrode was gently washed with PBS buffer and dried with ultrapure nitrogen.

https://dx.doi.org/10.1021/acsami.0c22062
ACS Appl. Mater. Interfaces 2021, 13, 4905−4914

Scheme 1. Schematic Representation of the Biosensor for *S. aureus* Based on a DNA Walker and DNA Nanoflowers

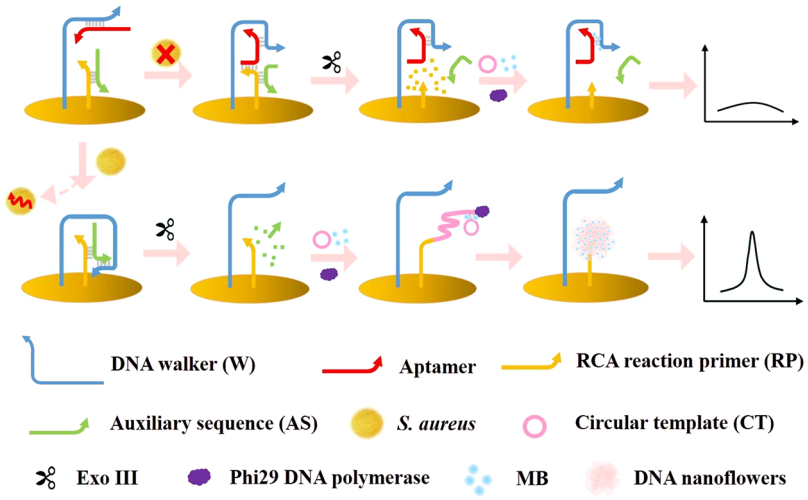

To prepare the circular DNA template for RCA reaction, T4 DNA ligase was used to catalyze the ligation of 5′ and 3′ terminals of a presynthesized ssDNA. T4 DNA ligase was first diluted to 40 U/μL with the accompanying buffer (50 mM Tris-HCl, 10 mM $MgCl_2$, 10 mM DTT, 1 mM ATP, pH 7.5). The circular reaction system (40 μL) contains 8 μL of 100 μM CT, 1 μL of diluted T4 DNA ligase, 4 μL of 10×T4 DNA ligase buffer, and 27 μL of ddH_2O. The reaction system was incubated at 16 °C for 12 h to complete the ligation. Finally, the solution was treated at 65 °C for 10 min to terminate the reaction, and the product was stored at 4 °C prior use.

A 2 μL aliquot of circular DNA was added to 10 μL of 10×phi29 DNA polymerase buffer, 1 μL of 10 U/μL phi29 DNA polymerase, 5 μL of 25 μM dNTPs, 10 μL of 2 mg/mL BSA, and 72 μL of MB solution to prepare overall 100 μL of an RCA reaction system. The reaction solution was dropped on the electrode surface and incubated at 30 °C for 3 h. Finally, the electrode was washed with PBS buffer to remove the reaction system and dried with ultrapure nitrogen.

To achieve the best detection effect, ultrapure nitrogen was used to remove oxygen dissolved in the PBS buffer for 30 min in advance. The modified gold electrode, platinum wire electrode, and Ag/AgCl electrode were inserted into the PBS buffer and correctly connected with the electrochemical workstation for DPV scanning. The scanning voltage was −0.5 to 0.1 V. The electrochemical impedance spectroscopy (EIS) was used to characterize the modification of the electrode. The electrode was placed in 0.1 mM $[Fe(CN)_6]^{3-/4-}$ solution (containing 0.1 M KCl) with a scanning frequency of 0.1 Hz−10 kHz.

2.5. Characterization of DNA Nanoflowers. DNA nanoflowers were characterized by field emission scanning electron microscopy (FESEM). First, the protective film was removed from the silicon wafer, and then the silicon wafer was soaked overnight in freshly prepared aqua regia (HNO_3:HCl = 1:3). Second, the silicon wafer was washed with anhydrous ethanol for three times, followed by washing with acetone for several times and drying. Then 5 μL of RCA reaction products was dropped to the center of the silicon wafer and dried in an oven at 28 °C for 2 h. Subsequently, it was washed with ddH_2O to desalinate and dried in the oven. Finally, the morphology of DNA sample was photographed by FESEM (SU8220, HITACHI, Japan). Because of the poor conductivity of DNA, it is necessary to spray platinum on the surface of the dried sample to increase its conductivity. The self-assembled structure of DNA nanoflowers was characterized under the excitation voltage of 3 kV.

2.6. Detection of *S. aureus* in Real Samples. To verify the performance of the biosensor in practical application, different concentrations of *S. aureus* were added to lake water, tap water, and honey samples (diluted 10 times with PBS buffer) to prepare artificially contaminated samples. The detection was performed under the optimum conditions as described above. The recovery rate and relative standard deviation (RSD) were calculated.

3. RESULTS AND DISCUSSION

3.1. Principle of the Electrochemical Detection of *S. aureus*. An electrochemical biosensor for *S. aureus* is constructed based on a DNA walker and DNA nanoflowers, and the signal release process of the DNA walker based on enzymatic catalysis on the electrode surface is explored. As shown in Scheme 1, the aptamer is partially complementary to W, and AS is partially complementary to RP. The thiol group is modified at the 5′ terminal of W and RP, so that the aptamer/W and AS/RP duplexes can be fixed on the surface of the electrode via Au−S bonds.

When *S. aureus* is present in the solution, it binds to the aptamer in the aptamer/W duplex, leaving single-stranded W on the electrode surface. Acting as the walker, W recognizes and hybridizes with the free 3′ terminal of AS in AS/RP duplex to form a hybridized complex. Under the catalysis of Exo III, AS in the complex is gradually hydrolyzed from its fully complementary 3′ terminal. Thus, the complex is disassembled, leaving single-stranded W and RP on the electrode surface. The free W can carry out walking process on the electrode surface and continue to hybridize with the unreacted AS/RP duplex and trigger the hydrolysis reaction, producing a large number of single-stranded RP. After the addition of circular DNA CT and phi29 DNA polymerase, RP is elongated continuously due to the RCA reaction, which greatly increases the local concentration of DNA in the solution; therefore, DNA nanoflowers form. Meanwhile, because of the complementary bases in the designed circular DNA template, a large number of complementary pairings occur in the long-strand RCA product. MB is a kind of low toxic organic dye with low molecular weight, which can interact with the DNA duplex through both electrostatic adsorption and intercalation binding. MB has redox activity and can shuttle electrons along the DNA duplex, thereby enhance the conductivity of DNA and generate a strong current response.[40,41] The Nupack online service was used to simulate the secondary structure of the elongated DNA strand after extending five circular templates (actual length far exceeds this simulated sequence). As can be seen in Figure S1, the extended DNA strand forms numerous double-stranded regions due to the complementary pairing.

https://dx.doi.org/10.1021/acsami.0c22062
ACS Appl. Mater. Interfaces 2021, 13, 4905−4914

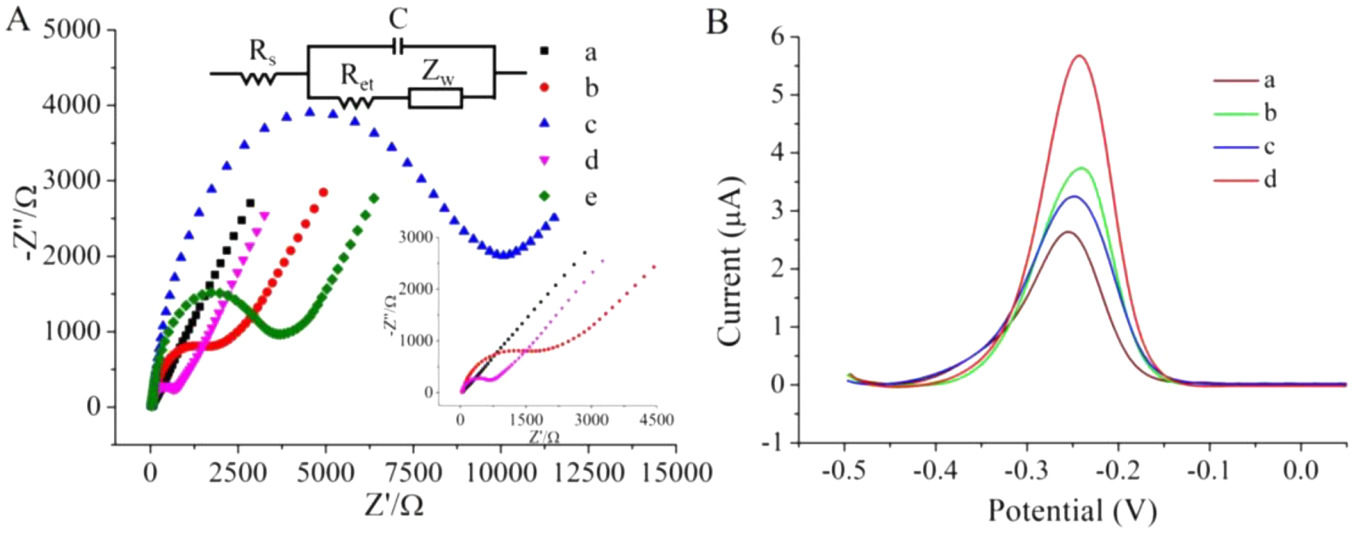

Figure 1. Characterization of electrode modification process. (A) EIS curves of each steps: (a) bare electrode; (b) electrode modified with aptamer/W and AS/RP duplexes; (c) electrode modified with aptamer/W and AS/RP duplexes and blocked with 6-MCH; (d) electrode modified with aptamer/W and AS/RP duplexes, blocked with 6-MCH and digested by Exo III; (e) electrode modified with aptamer/W and AS/RP duplexes, blocked with 6-MCH, digested by Exo III, and elongated by phi29 DNA polymerase. Inset shows an enlarged view of curves a, b, and d. EIS was modeled by using the Randle's equivalent circuit: C is the interfacial double-layer capacitance, R_s is the solution resistance, R_{et} is the electron transfer resistance, and Z_w is the Warburg impedance. (B) DPV curves: (a) reaction without phi29 DNA polymerase; (b) reaction without Exo III; (c) PBS control; (d) experimental group.

The electroactive MB embedded in double strands produces an intensive electrochemical signal, and thus the concentration of *S. aureus* can be calculated by measuring the current response of the electrode.

When *S. aureus* is absent in the solution, the aptamer/W and AS/RP duplexes can further hybridize to form a complex because the 5′ terminal of the aptamer is complementary to the 3′ terminal of the RP. Under the catalysis of Exo III, RP is hydrolyzed and the complex is disassembled. The released aptamer/W duplex can continuously hybridize with the unreacted AS/RP duplex and hydrolyze RP. The RCA reaction cannot occur without RP, and thus only a low electrochemical signal can be detected.

3.2. Feasibility of the Proposed Strategy for *S. aureus* Detection. First, the electrode modification process was characterized by EIS. The electrostatic repulsion between $Fe(CN)_6^{4-/3-}$ and the negatively charged phosphoric acid backbone modified on the electrode surface prevents the electron transfer between $Fe(CN)_6^{4-/3-}$ and the electrode, thus increasing the electron transfer resistance (R_{et}). In the EIS diagram, the diameter of the semicircle represents R_{et}; that is, the larger diameter means a higher R_{et} value. As shown in Figure 1A, R_{et} of the bare gold electrode is very low, and the EIS curve is almost linear (curve a, black in the inset). When the aptamer/W and AS/RP duplexes are modified on the electrode surface, R_{et} apparently increases (curve b, red in the inset). After the excess sites on the electrode surface are blocked with 6-MCH, R_{et} of the electrode further increases (curve c). Exo III is used to regenerate the DNA walker by digesting part of the DNA sequences, which reduces R_{et} caused by the electrostatic repulsion of phosphate backbone on the electrode surface (curve d). Interestingly, Exo III may have a certain effect on the blocking of 6-MCH on the electrode surface; thus, R_{et} in EIS decreases sharply (verified in the Supporting Information and Figure S2). Finally, the RCA reaction catalyzed by phi29 DNA polymerase significantly elongates the length of RP and increases the content of phosphate backbone on the electrode surface, leading to the increased R_{et} (curve e).

The constructed electrochemical biosensor involves two-step enzyme reactions: Exo III digestion reaction and RCA reaction. Exo III digestion is used to realize the walking process of DNA walker on the electrode surface. Phi29 DNA polymerase is used to produce a large number of elongated single-stranded DNA to form DNA nanoflowers, which provides binding sites for electroactive MB and thus amplifies the signal. To characterize the mechanism of the detection, DPV curves were recorded under different conditions. The concentrations of Aptamer/W and AS/RP were fixed at 100 and 500 nM, respectively. As shown in Figure 1B, a high peak current is observed in DPV when *S. aureus* (6×10^8 CFU/mL), Exo III (10 U), and phi29 DNA polymerase (8 U) are present in the reaction system. However, the absence of either *S. aureus*, Exo III, or phi29 DNA polymerase leads to a weak peak current in DPV. In the PBS control group, aptamer/W as a whole hybridizes with AS/RP through the partially complementary region between the aptamer and RP. Then Exo III starts hydrolyzation from the 3′ terminal of the fully complementary RP. Because of the lack of primers, the RCA reaction cannot be achieved. Therefore, curve c shows the background signal of the aptamer/W duplex remaining on the electrode surface. When *S. aureus* exists in solution, the aptamer binds to *S. aureus* and W is released. The 3′ terminal of W complements to AS, and then AS is hydrolyzed from the 3′ terminal by Exo III. If there is no phi29 DNA polymerase in the solution, the RCA reaction cannot take place. Curve a shows the background signal caused by W and RP single strands. However, when Exo III is not present in the solution, the hydrolysis cannot take place. The polymerase added subsequently elongates the complementary AS/W, and curve b shows the background signal when MB is embedded in AS/W and AS/RP. Obviously, both Exo III and phi29 DNA polymerase are indispensable for the constructed biosensor.

https://dx.doi.org/10.1021/acsami.0c22062
ACS Appl. Mater. Interfaces 2021, 13, 4905−4914

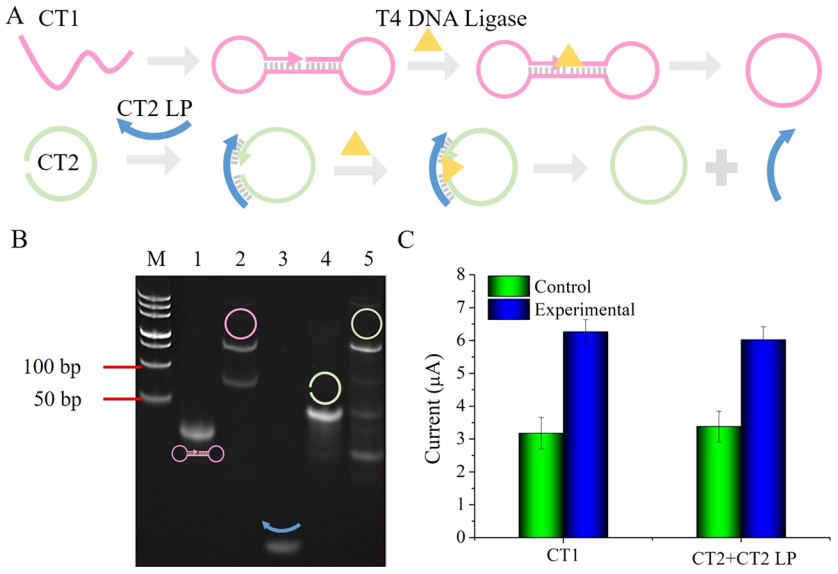

Figure 2. Effect of different circular DNA on signal response. (A) Schematic diagram of two different strategies to form circular DNA. (B) PAGE image of circular DNA formation. Lane M: DNA marker; lane 1: linear CT1 (5 μM); lane 2: circular CT1 (5 μM); lane 3: CT2 LP (5 μM); lane 4: linear CT2 (5 μM); lane 5: circular CT2 (5 μM). (C) Effect of different circular DNA on detection.

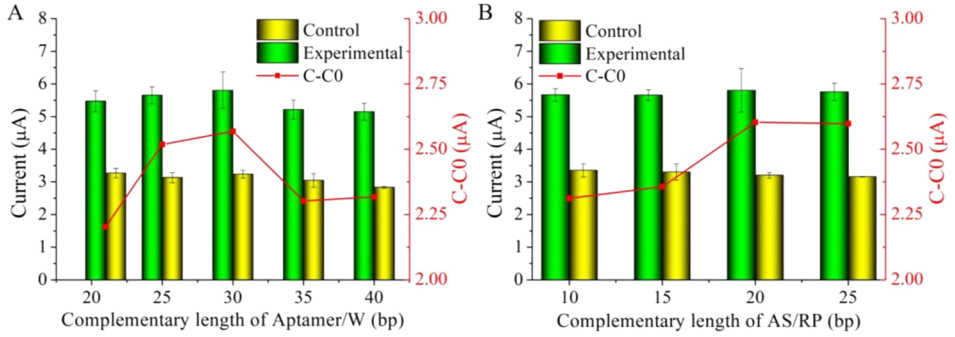

Figure 3. (A) Relationship between the current response and the length of complementary region in aptamer/W. (B) Relationship between the current response and the length of the complementary region in AS/RP. *C* represents the current response of the experimental group, and *C*0 represents the current response of the control group.

Thus, the modification and reaction process of the electrode are well characterized.

3.3. Design of Circular DNA. To prepare circular DNA, a phosphate group was modified at the 5′ terminal of CT, and T4 DNA ligase was used to ligate the two terminals of the single-stranded DNA to form a circular structure. As shown in Figure 2A, there are mainly two strategies to prepare circular DNA. One is to make the 5′ and 3′ terminals of the single-stranded DNA close to each other through the formation of the secondary structure by DNA itself (self-cyclization strategy). The other is to hybridize the single-stranded DNA to the corresponding primer to make its 5′ and 3′ terminals close to each other (primer-based cyclization strategy). To compare the efficiency of two different ways to prepare the circular DNA, self-cyclization padlock (CT1), primer-based cyclization padlock (CT2), and CT2 ligation primer (LP) were designed, and the sequences are shown in Table S1.

The migration rate of linear DNA in polyacrylamide gel electrophoresis (PAGE) is inversely proportional to the molecular weight of DNA. The migration rate of circular DNA is slightly higher than that of linear DNA with the same molecular weight. However, when gel concentration is relatively high, circular DNA cannot enter the gel, and the mobility decreases greatly. Therefore, linear DNA and circular DNA with the equivalent molecular weight can be clearly distinguished by using high-concentration PAGE. Herein, 12% PAGE was used to verify the formation of circular DNA, and the detailed methods can be found in the Supporting Information. As shown in Figure 2B, lanes 1, 3, and 4 represent CT1, CT2 LP, and CT2, respectively. Lanes 2 and 5 are the corresponding circular DNAs. The results show that both methods can form ideal circular DNA.

To further compare the performance of circular DNA prepared by different ways, the two circular DNAs were employed to construct the biosensors. As shown in Figure 2C, the green columns are the current responses of the control groups without *S. aureus*, and the blue columns are the current responses of the experimental groups with the same concentration of *S. aureus*. Compared with the CT2 groups, the signal difference of CT1 groups increases by 16.69%. The results show that when circular DNA prepared through self-cyclization is used in the biosensor, the difference of current response between the experimental group and the control group is the higher, which indicates the better detection performance. Therefore, CT1 is selected as the circular DNA in this study.

https://dx.doi.org/10.1021/acsami.0c22062
ACS Appl. Mater. Interfaces 2021, 13, 4905−4914

3.4. Optimization of the Length of Complementary Regions in Aptamer/W and AS/RP Duplexes. The aptamer/W duplex acts as the primary response element in the biosensor configuration. After the incubation of aptamer/W with *S. aureus*, the aptamer competitively binds to *S. aureus*, which makes the aptamer release from the double strand. The single-stranded W hybridizes with AS/RP duplex to induce the hydrolysis of AS with the help of Exo III. If the complementary region of the aptamer and W is too long, the combination of the aptamer and W will hinder the binding of *S. aureus* with the aptamer. On the contrary, a too short complementary region between the aptamer and W will affect the stability of double-stranded structure. The primer in AS/RP is used to provide the binding site of circular DNA and initiate the RCA reaction. If the complementary region of the AS/RP duplex is too short, the stability of the duplex will be low, and thus it is easy to expose the primer in advance when there is no target in the system, resulting in high background signal. Therefore, the lengths of complementary regions in aptamer/W and AS/RP duplexes were optimized, and the sequences are shown in Table S1.

To investigate the effect of the length of complementary region of aptamer/W, it is designed to be 20, 25, 30, 35, and 40 bp. The corresponding biosensors are constructed to detect the samples with or without *S. aureus*. The detection performance is assessed by the difference between C and $C0$, which represent the peak current of the experimental group and the control group, respectively. As shown in Figure 3A, with the increase of the length of complementary region, the peak current of the experimental group increases. When the length exceeds 30 bp, the peak current decreases gradually. For the control group, the peak current decreases slightly with the increase of the complementary length. It can be speculated that with the increase of the length of complementary region the double-stranded structure tends to be stable, which leads to the increase of the amount of double strands modified on the electrode surface and the subsequent current response. However, the further increase of the complementary length influences the binding of the aptamer with the target; thus, the peak current decreases slightly. Therefore, the aptamer/W duplex with the 30 bp complementary region is selected.

To obtain the ideal AS/template duplex, the length of complementary region of AS/RP duplex is designed to be 10, 15, 20, and 25 bp and used in the constructed biosensor for *S. aureus*. As can be seen in Figure 3B, the change of the length of complementary region of AS/RP duplex has little effect on the current response of the experimental group. However, the peak current of the control group decreases slightly and tends to be stable when the length of complementary region increases. According to the value of $C - C0$, the optimal detection result is achieved when the length of complementary region of AS/RP is 20 bp.

3.5. Ratio of Aptamer/W and AS/RP Duplexes. The aptamer/W duplex is incubated with the target to release W. With the help of Exo III, W acts as DNA walker to hybridize and subsequently digest the AS/RP duplex, which releases the free primer for RCA reaction. The detection sensitivity is related to the ratio of aptamer/W and AS/RP duplexes. If the concentration of AS/RP is too low, the amount of RP released by Exo III hydrolysis becomes less, which cannot achieve effective signal amplification. If the concentration of AS/RP is too high, it will produce steric hindrance on the electrode surface, which will affect the follow-up reaction. Therefore, to optimize the ratio of the two duplexes, the addition ratio of aptamer/W and AS/RP duplexes is set to be 1:1, 1:2, 1:4, 1:5, and 1:10. As shown in Figure S3, with the increase of AS/RP, the peak current of the control group increases slightly. The peak current of the experimental group decreases slightly after the addition ratio is lower than 1:5. According to the value of $C - C0$, when the addition ratio of aptamer/W and AS/RP is 1:5, the detection performance of the biosensor is the best.

3.6. Optimization of the Experimental Parameters. To obtain the optimal detection performance of the biosensor, the amount of Exo III, the reaction time of Exo III, the amount of phi29DNA polymerase, and RCA reaction time were optimized. The experiments were performed at the fixed *S. aureus* concentration of 6×10^8 CFU/mL. Among them, the optimization of the amount and reaction time of Exo III takes the peak current of the experimental groups as the evaluation index. However, the signal growth rate is employed as the evaluation index during the optimization of the amount of phi29 DNA polymerase and RCA reaction time to complete the detection in reasonable time with low cost.

The regeneration and walking of DNA walker on the electrode surface depend on the digestion of AS in the multistranded hybridized complex by Exo III. If the concentration of Exo III is too low, the walking and subsequent signal amplification process will be restricted, while too high concentration of Exo III will cause unnecessary waste. Therefore, different amounts of Exo III ranging from 5 to 15 U were used for the digestion reaction, and the rest of the detection conditions remained unchanged. As shown in Figure S4A, when the added enzyme increases from 5 to 7.5 U, the peak current increases significantly and then decreases slightly. So the optimum amount of Exo III is 7.5 U.

The regeneration of the DNA walker is not only dependent on the amount of Exo III but also related to the digestion time. As shown in Figure S4B, the reaction time was adjusted from 40 to 120 min while the rest of the detection conditions were unchanged. The peak current reaches the highest when the reaction time of Exo III is 100 min.

Phi29 DNA polymerase is used to catalyze RCA reaction to produce a large number of long DNA strands. When the concentration of local DNA strands in the solution is high, the strands complement with each other and crystallize to form DNA nanoflowers. The amount of phi29 DNA polymerase affects the rate of RCA reaction and the formation of DNA nanoflowers. As shown in Figure S4C, the peak current increases with the increase of the amount of the enzyme. By calculating the signal growth rate $((C_{n+1} - C_n)/C_n \times 100\%)$, it is found that with the increase of the polymerase the signal growth rate decreases. When the addition of phi29 DNA polymerase reaches 7.5 U, the signal growth rate reaches the maximum. Therefore, the optimal amount of phi29 DNA polymerase is 7.5 U.

The amplification efficiency of RCA reaction is related to not only the amount of phi29 DNA polymerase but also the reaction time. As shown in Figure S4D, with the extension of the RCA reaction time, the peak current increases continuously. When the reaction time is 3 h, the signal growth rate is the highest. Therefore, the optimal RCA reaction time is 3 h.

3.7. Characterization of the DNA Nanoflowers. DNA nanoflowers are formed by self-assembly and liquid crystallization of a high concentration of DNA. Compared with the traditional DNA nanostructure, the assembly of DNA nanoflowers does not depend on the DNA sequence, which

https://dx.doi.org/10.1021/acsami.0c22062
ACS Appl. Mater. Interfaces 2021, 13, 4905−4914

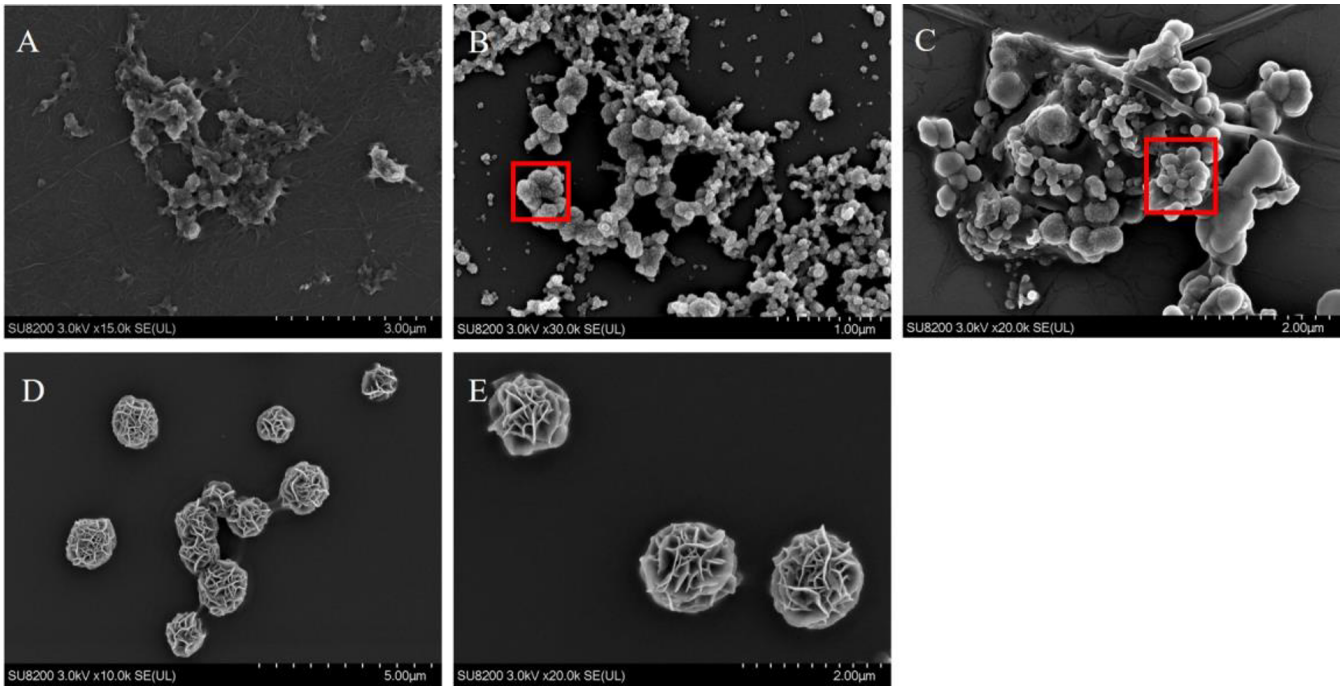

Figure 4. FESEM of DNA nanoflowers produced by RCA reaction with different RCA reaction times: (A) 1, (B) 3, (C) 5, (D) 7, and (E) 9 h. The patterns in the red box of (B) and (C) are the embryonic form of DNA nanoflowers.

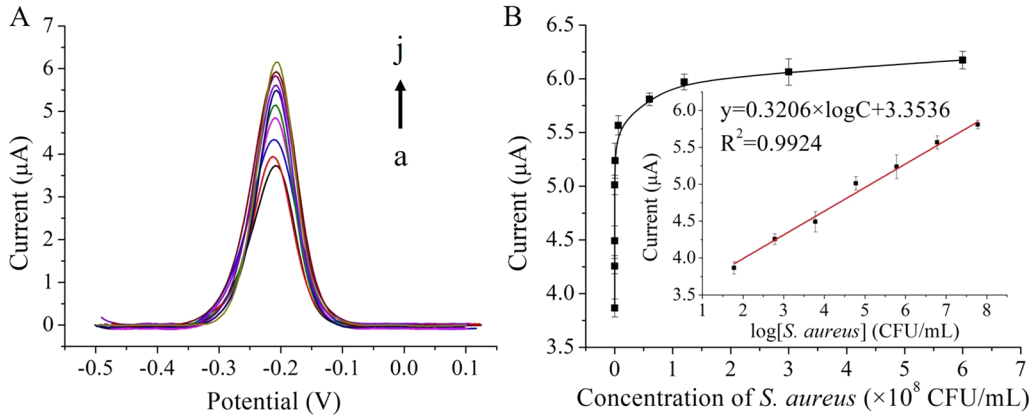

Figure 5. (A) DPV curves recorded at different concentrations of *S. aureus*: (a) 60, (b) 6×10^2, (c) 6×10^3, (d) 6×10^4, (e) 6×10^5, (f) 6×10^6, (g) 6×10^7, (h) 1.2×10^8, (i) 3×10^8, and (j) 6×10^8 CFU/mL. (B) Relationship between the current response and the concentration of *S. aureus*. The inset shows the linear relationship between the current response and the logarithm of *S. aureus* concentration.

avoids the complicated design of DNA. In the constructed sensor, the formation of DNA nanoflowers provides sufficient binding sites for electroactive MB and intensively increases the current response.

To directly characterize the formation of DNA nanoflowers in solution, the RCA reaction products with different reaction time were photographed by FESEM. As shown in Figure 4, panels A–E are the SEM images of products after RCA reaction for 1–9 h. After 1 h RCA reaction, DNA strands in the solution is not enough to be self-assembled to form DNA nanoflowers. When the reaction time is extended to 3 h, the DNA strands increase and begin to aggregate. The DNA nanoflowers can be identified, with the particle size of about 0.3 μm. When the reaction time reaches 5 h, with the larger DNA aggregation products in the solution, some relatively clear DNA nanoflowers with particle size of about 0.8 μm can be observed. From the patterns in the red boxes in Figures 4B and 4C, it can be seen that the DNA strands begin to gather, and the embryonic form of DNA nanoflowers appears. When the reaction time is further extended to 7–9 h, the DNA nanoflowers with uniform particle sizes can be seen in the solution. The average particle size of DNA nanoflowers is about 1 μm after 7 h reaction and 1.3 μm after 9 h reaction. The results of FESEM well characterize the formation of DNA nanoflowers in the solution with different RCA reaction times.

With the extension of the reaction time, the concentration of local DNA in the solution increases, and the DNA nanoflowers thus form. At the same time, DNA crystallizes and forms a gel-like structure. As shown in Figure S5, with the continuous extension of the RCA reaction time, the particle size of DNA nanoflowers continues to increase, and a light milky white gel-like substance appears in the solution. The formation of the gel-like substance is also the evidence of the formation of DNA nanoflowers.

https://dx.doi.org/10.1021/acsami.0c22062
ACS Appl. Mater. Interfaces 2021, 13, 4905–4914

3.8. Performance of the Electrochemical Biosensor. A 100 μL aliquot of different concentrations of *S. aureus* was added to the electrode reaction system for investigation of the sensitivity and dynamic response range of the biosensor. Under the optimal detection conditions, the change of current response caused by different concentration of *S. aureus* was recorded.

As shown in Figure 5, in the concentration range from 60 to 6×10^8 CFU/mL, the peak current in DPV increases with the increase of the concentration of *S. aureus*. Furthermore, a linear relationship is derived between the current response and the logarithm of *S. aureus* concentration from 60 to 6×10^7 CFU/mL (Figure 5B, inset). The linear regression equation is $y = 0.3206 \times \log C + 3.3536$ ($R^2 = 0.9924$), where y indicates the peak current (μA) and C indicates the concentration of *S. aureus* (CFU/mL). The detection limit is calculated to be 9 CFU/mL (S/N = 3). The biosensor achieves dual-signal amplification through the action of DNA walker and the self-assembly of DNA nanoflowers. Compared with other electrochemical aptasensors for *S. aureus* listed in Table 1, the sensitivity and the dynamic response range of the biosensor in this work are comparable to those high performance sensors.

Table 1. Comparison of the Proposed Assay with Previous Electrochemical Aptasensor for *S. aureus*

substrate	technique	LOD (CFU/mL)	linear range (CFU/mL)	ref
rGO-AuNP/GCE	electrochemical impedance spectroscopy	10	$10-10^6$	42
redox-active gold nanoparticles	cyclic voltammetry	10	$10-10^5$	43
aptamer/AuE	electrochemical impedance spectroscopy	10	$1-10^9$	44
AuNPs/CS-MWCNTs/AuE	differential pulse voltammetry	10	$10-10^6$	45
apt/*S. aureus*/apt-AgNPs/magnetic beads	differential pulse voltammetry	1	$10-10^6$	46
MB/DNA nanoflowers/AuE	differential pulse voltammetry	9	$60-6 \times 10^7$	this work

Several common nontarget bacteria samples such as *E. faecium*, *L. monocytogenes*, *P. aeruginosa*, *E. faecalis*, *S. enteritidis*, and the mixed bacteria samples were used to investigate the specificity of the biosensor. As shown in Figure 6, when the biosensor is used to detect *S. aureus*, the current response is significantly higher than those of other nontarget samples, indicating that the biosensor has good specificity. The mixed bacterial samples were prepared by mixing the same concentration of *S. aureus* with other nontarget bacteria, and the sensor was used to determine *S. aureus* in the mixed bacterial solution. Because of the existence of interferents in the mixed bacterial solution, the signal response is slightly higher than that of the standard *S. aureus* sample. The results show that the biosensor has good potential in the detection of *S. aureus* in complicated samples.

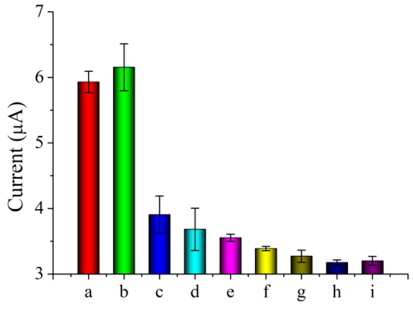

Figure 6. Verification of the specificity of biosensor: (a) *S. aureus*, (b) mixture of seven bacteria including *S. aureus*, (c) *E. faecium*, (d) *L. monocytogenes*, (e) *P. aeruginosa*, (f) *E. coli*, (g) *E. faecalis*, (h) *S. enteritidis*, and (i) PBS control. The concentrations are 3×10^8 CFU/mL for *S. aureus* and 3×10^9 CFU/mL for other bacteria.

3.9. Detection of *S. aureus* in Real Samples. To evaluate the practicability of the constructed biosensor in detecting actual samples, several bacteria-contaminated samples were prepared. To eliminate the potential influence of *S. aureus* which originally exists in the actual samples, certain concentrations of *S. aureus* were spiked to the sterilized and filtered lake water, tap water, and diluted honey sample. All the testing conditions are the same as those for the standard samples and measured for three times. As shown in Table 2,

Table 2. Detection of *S. aureus* in Real Samples (n = 3)

samples	added (CFU/mL)	detected (CFU/mL)	recovery (%)	RSD (%)
lake water 1	6.00×10^4	6.32×10^4	105.30	1.07
lake water 2	6.00×10^7	6.37×10^7	106.21	1.87
tap water 1	6.00×10^4	6.23×10^4	103.80	3.21
tap water 2	6.00×10^7	6.10×10^7	101.73	2.18
diluted honey 1	6.00×10^4	5.97×10^4	99.42	1.70
diluted honey 2	6.00×10^7	5.68×10^7	94.68	4.45

the recovery of the actual samples is in the range 94.7−106.2%, and the relative standard deviation (RSD) is in the range 1.07−4.45%, indicating that the biosensor has excellent practicability.

4. CONCLUSION

The unique design in this work integrates the superiority of DNA nanodevice and the response elements to construct an electrochemical biosensor for *S. aureus*. The biosensor realizes the walking process of DNA walker on the electrode surface under the digestion of Exo III. RCA reaction increases the local concentration of DNA in the solution and produces the DNA nanoflowers, which provide sufficient binding sites for MB and amplify the detection signal. A broad dynamic response range within $60-6 \times 10^8$ CFU/mL is derived, and the detection limit is 9 CFU/mL. At the same time, the biosensor has high specificity and good interferent resistance, which can distinguish *S. aureus* from other nontarget bacteria in the mixed samples. In addition, the assay has been used to detect the *S. aureus* in real water samples and diluted honey samples, indicating that it has great potential in environmental monitoring and food safety. Moreover, the one-step preparation of DNA nanoflowers in the biosensor configuration is much simpler than the construction of other DNA nanostructures. The biosensor surely faces many challenges at present. The detection system is relatively complex, which makes it not suitable for on-site rapid detection. However, with the continuous progress of sensing technology, its future application can be expected. By replacing the loaded signal molecules, we can use the design in biological imaging, intracellular determination, and other fields.

https://dx.doi.org/10.1021/acsami.0c22062
ACS Appl. Mater. Interfaces 2021, 13, 4905−4914

■ ASSOCIATED CONTENT

Supporting Information

The Supporting Information is available free of charge at https://pubs.acs.org/doi/10.1021/acsami.0c22062.

Experimental details of 12% PAGE for circular DNA formation; experimental details of the effect of Exo III on the MCH blocked electrode; table of all oligonucleotide sequences used in this experiment (Table S1); the secondary structure of the extended DNA strand after extending five circular templates (Figure S1); EIS diagram for the effect of Exo III on the blocking process of electrode surface (Figure S2); current response for the different ratio of aptamer/W and AS/RP modified on the electrodes (Figure S3); optimization of Exo III concentration, the reaction time for Exo III, phi29 DNA polymerase concentration, the reaction time for RCA (Figure S4); FESEM images of DNA nanoflowers after 7 and 9 h RCA reaction; photos of the gel-like substance after 7 and 9 h RCA reaction (Figure S5) (PDF)

■ AUTHOR INFORMATION

Corresponding Authors

Maolin Li − *Department of Laboratory Medicine, Yixing Tumor Hospital, Yixing 214200, China*; Email: 13961511114@163.com

Nandi Zhou − *The Key Laboratory of Carbohydrate Chemistry and Biotechnology, Ministry of Education, School of Biotechnology, Jiangnan University, Wuxi 214122, China*; orcid.org/0000-0002-2906-7781; Email: zhounandi@jiangnan.edu.cn

Authors

Rongfeng Cai − *The Key Laboratory of Carbohydrate Chemistry and Biotechnology, Ministry of Education, School of Biotechnology, Jiangnan University, Wuxi 214122, China*

Shixin Zhang − *The Key Laboratory of Carbohydrate Chemistry and Biotechnology, Ministry of Education, School of Biotechnology, Jiangnan University, Wuxi 214122, China*

Luo Chen − *The Key Laboratory of Carbohydrate Chemistry and Biotechnology, Ministry of Education, School of Biotechnology, Jiangnan University, Wuxi 214122, China*

Yuting Zhang − *The Key Laboratory of Carbohydrate Chemistry and Biotechnology, Ministry of Education, School of Biotechnology, Jiangnan University, Wuxi 214122, China*

Complete contact information is available at: https://pubs.acs.org/10.1021/acsami.0c22062

Notes

The authors declare no competing financial interest.

■ ACKNOWLEDGMENTS

This research was supported by the Six Talent Peaks Project in Jiangsu Province (JY-078) and the Postgraduate Research & Practice Innovation Program of Jiangsu Provence (KYCX18_1799).

■ ABBREVIATIONS

S. aureus, *Staphylococcus aureus*; Exo III, exonuclease III; RCA, rolling circle amplification; MB, methylene blue; 6-MCH, 6-mercaptohexanol; RP, rolling circle amplification reaction primer; W, walker sequence; AS, auxiliary sequence; CT, circular template sequence; *E. faecium*, *Enterococcus faecium*; *L. monocytogenes*, *Listeria monocytogenes*; *E. faecalis*, *Enterococcus faecalis*; *S. enteritidis*, *Salmonella enteritidis*; FESEM, field emission scanning electron microscope; RSD, relative standard deviation; R_{et}, electron transfer resistance; CT1, self-cyclization padlock; CT2, primer-based cyclization padlock; LP, CT2 ligation primer; PAGE, polyacrylamide gel electrophoresis.

■ REFERENCES

(1) Liu, P.; Qian, X.; Li, X.; Fan, L.; Li, X.; Cui, D.; Yan, Y. Enzyme-Free Electrochemical Biosensor Based on Localized DNA Cascade Displacement Reaction and Versatile DNA Nanosheets for Ultrasensitive Detection of Exosomal MicroRNA. *ACS Appl. Mater. Interfaces* **2020**, *12*, 45648−45656.

(2) Li, D.; Li, X.; Yang, F.; Yuan, R.; Xiang, Y. Targeted Delivery of DNA Framework-Encapsulated Native Therapeutic Protein into Cancer Cells. *ACS Appl. Mater. Interfaces* **2020**, *12*, 54489−54496.

(3) Zhang, Y.; Tu, J.; Wang, D.; Zhu, H.; Maity, S. K.; Qu, X.; Bogaert, B.; Pei, H.; Zhang, H. Programmable and Multifunctional DNA-Based Materials for Biomedical Applications. *Adv. Mater.* **2018**, *30*, e1703658.

(4) Zhu, B.; Wang, L.; Li, J.; Fan, C. Precisely Tailored DNA Nanostructures and Their Theranostic Applications. *Chem. Rec.* **2017**, *17*, 1213−1230.

(5) Kong, G.; Zhang, M.; Xiong, M.; Fu, X.; Ke, G.; Zhang, X.-B. DNA Nanostructure-Based Fluorescent Probes for Cellular Sensing. *Anal. Methods* **2020**, *12*, 1415−1429.

(6) Zhou, X.; Zhao, M.; Duan, X.; Guo, B.; Cheng, W.; Ding, S.; Ju, H. Collapse of DNA Tetrahedron Nanostructure for "Off-On" Fluorescence Detection of DNA Methyltransferase Activity. *ACS Appl. Mater. Interfaces* **2017**, *9*, 40087−40093.

(7) Sun, J.; Sun, X. Recent Advances in the Construction of DNA Nanostructure with Signal Amplification and Ratiometric Response for MiRNA Sensing and Imaging. *TrAC, Trends Anal. Chem.* **2020**, *127*, 115900.

(8) Chandrasekaran, A. R.; Punnoose, J. A.; Zhou, L.; Dey, P.; Dey, B. K.; Halvorsen, K. DNA Nanotechnology Approaches for MicroRNA Detection and Diagnosis. *Nucleic Acids Res.* **2019**, *47*, 10489−10505.

(9) Wu, T.; Liu, Q.; Cao, Y.; Tian, R.; Liu, J.; Ding, B. Multifunctional Double-Bundle DNA Tetrahedron for Efficient Regulation of Gene Expression. *ACS Appl. Mater. Interfaces* **2020**, *12*, 32461−32467.

(10) Tripathy, N.; Kim, D. H. Metal Oxide Modified ZnO Nanomaterials for Biosensor Applications. *Nano Converg.* **2018**, *5*, 27.

(11) Ji, J.; Pang, Y.; Li, D.; Wang, X.; Xu, Y.; Mu, X. Single-Layered Graphene/Au-Nanoparticles-Based Love Wave Biosensor for Highly Sensitive and Specific Detection of *Staphylococcus aureus* Gene Sequences. *ACS Appl. Mater. Interfaces* **2020**, *12*, 12417−12425.

(12) Keller, A.; Linko, V. Challenges and Perspectives of DNA Nanostructures in Biomedicine. *Angew. Chem., Int. Ed.* **2020**, *59*, 15818−15833.

(13) Chai, H.; Miao, P. Bipedal DNA Walker based Electrochemical Genosensing Strategy. *Anal. Chem.* **2019**, *91*, 4953−4957.

(14) Chen, J.; Luo, Z.; Sun, C.; Huang, Z.; Zhou, C.; Yin, S.; Duan, Y.; Li, Y. Research Progress of DNA Walker and Its Recent Applications in Biosensor. *TrAC, Trends Anal. Chem.* **2019**, *120*, 115626.

(15) Huang, J.; Zhu, L.; Ju, H.; Lei, J. Telomerase Triggered DNA Walker with A Superhairpin Structure for Human Telomerase Activity Sensing. *Anal. Chem.* **2019**, *91*, 6981−6985.

(16) Mason, S. D.; Tang, Y.; Li, Y.; Xie, X.; Li, F. Emerging Bioanalytical Applications of DNA Walkers. *TrAC, Trends Anal. Chem.* **2018**, *107*, 212−221.

(17) Chen, F.; Xue, J.; Bai, M.; Qin, J.; Zhao, Y. Programming in Situ Accelerated DNA Walkers in Diffusion-Limited Microenvironments. *Chem. Sci.* **2019**, *10*, 3103−3109.

(18) Thavarajah, W.; Silverman, A. D.; Verosloff, M. S.; Kelley-Loughnane, N.; Jewett, M. C.; Lucks, J. B. Point-Of-Use Detection of

Environmental Fluoride via A Cell-Free Riboswitch-Based Biosensor. *ACS Synth. Biol.* **2020**, *9*, 10−18.
(19) Zhang, R.; Wang, Y.; Qu, X.; Li, S.; Zhao, Y.; Liu, S.; Huang, J. Exonuclease III-Powered DNA Walking Machine for Label-Free and Ultrasensitive Electrochemical Sensing of Antibiotic. *Sens. Actuators, B* **2019**, *297*, 126771.
(20) Wang, D.; Vietz, C.; Schröder, T.; Acuna, G.; Lalkens, B.; Tinnefeld, P. A DNA Walker as A Fluorescence Signal Amplifier. *Nano Lett.* **2017**, *17*, 5368−5374.
(21) Hu, R.; Zhang, X.; Zhao, Z.; Zhu, G.; Chen, T.; Fu, T.; Tan, W. DNA Nanoflowers for Multiplexed Cellular Imaging and Traceable Targeted Drug Delivery. *Angew. Chem., Int. Ed.* **2014**, *53*, 5821−5826.
(22) Mei, L.; Zhu, G.; Qiu, L.; Wu, C.; Chen, H.; Liang, H.; Cansiz, S.; Lv, Y.; Zhang, X.; Tan, W. Self-Assembled Multifunctional DNA Nanoflowers for the Circumvention of Multidrug Resistance in Targeted Anticancer Drug Delivery. *Nano Res.* **2015**, *8*, 3447−3460.
(23) Li, S. K.; Chen, A. Y.; Niu, X. X.; Liu, Z. T.; Du, M.; Chai, Y. Q.; Yuan, R.; Zhuo, Y. In Situ Generation of Electrochemiluminescent DNA Nanoflowers as A Signal Tag for Mucin 1 Detection Based on A Strategy of Target and Mimic Target Synchronous Cycling Amplification. *Chem. Commun.* **2017**, *53*, 9624−9627.
(24) Jin, Y.; Li, Z.; Liu, H.; Chen, S.; Wang, F.; Wang, L.; Li, N.; Ge, K.; Yang, X.; Liang, X.-J.; Zhang, J. Biodegradable, Multifunctional Dnazyme Nanoflowers for Enhanced Cancer Therapy. *NPG Asia Mater.* **2017**, *9*, e365.
(25) Lv, Y.; Hu, R.; Zhu, G.; Zhang, X.; Mei, L.; Liu, Q.; Qiu, L.; Wu, C.; Tan, W. Preparation and Biomedical Applications of Programmable and Multifunctional DNA Nanoflowers. *Nat. Protoc.* **2015**, *10*, 1508−1524.
(26) Shi, L.; Mu, C.; Gao, T.; Chen, T.; Hei, S.; Yang, J.; Li, G. DNA Nanoflower Blooms in Nanochannels: A New Strategy for MiRNA Detection. *Chem. Commun.* **2018**, *54*, 11391−11394.
(27) Chen, X.; Huang, J.; Zhang, S.; Mo, F.; Su, S.; Li, Y.; Fang, L.; Deng, J.; Huang, H.; Luo, Z.; Zheng, J. Electrochemical Biosensor for DNA Methylation Detection through Hybridization Chain-Amplified Reaction Coupled with A Tetrahedral DNA Nanostructure. *ACS Appl. Mater. Interfaces* **2019**, *11*, 3745−3752.
(28) Bocanegra-Rodriguez, S.; Jornet-Martinez, N.; Molins-Legua, C.; Campins-Falco, P. New Reusable Solid Biosensor with Covalent Immobilization of the Horseradish Peroxidase Enzyme: in Situ Liberation Studies of Hydrogen Peroxide by Portable Chemiluminescent Determination. *ACS Omega* **2020**, *5*, 2419−2427.
(29) Salinas Dominguez, R. A.; Dominguez Jimenez, M. A.; Orduna Diaz, A. Antibody Immobilization in Zinc Oxide Thin Films as an Easy-Handle Strategy for *Escherichia coli* Detection. *ACS Omega* **2020**, *5*, 20473−20480.
(30) Du, Y.; Dong, S. Nucleic Acid Biosensors: Recent Advances and Perspectives. *Anal. Chem.* **2017**, *89*, 189−215.
(31) Rouf, T. B.; Díaz-Amaya, S.; Stanciu, L.; Kokini, J. Application of Corn Zein as an Anchoring Molecule in a Carbon Nanotube Enhanced Electrochemical Sensor for the Detection of Gliadin. *Food Control* **2020**, *117*, 107350.
(32) Xue, L.; Huang, F.; Hao, L.; Cai, G.; Zheng, L.; Li, Y.; Lin, J. A Sensitive Immunoassay for Simultaneous Detection of Foodborne Pathogens Using MnO_2 Nanoflowers-Assisted Loading and Release of Quantum Dots. *Food Chem.* **2020**, *322*, 126719.
(33) Gao, R.; Lu, D.; Guo, D.; Xin, X. Dual-Optofluidic Waveguide In-Line Fiber Biosensor for Real-Time Label-Free Detection of Interferon-Gamma with Temperature Compensation. *Opt. Express* **2020**, *28*, 10491−10504.
(34) Loi, V. V.; Harms, M.; Muller, M.; Huyen, N. T. T.; Hamilton, C. J.; Hochgrafe, F.; Pane-Farre, J.; Antelmann, H. Real-Time Imaging of the Bacillithiol Redox Potential in the Human Pathogen *Staphylococcus aureus* Using A Genetically Encoded Bacilliredoxin-Fused Redox Biosensor. *Antioxid. Redox Signaling* **2017**, *26*, 835−848.
(35) Eissa, S.; Zourob, M. A Dual Electrochemical/Colorimetric Magnetic Nanoparticle/Peptide-Based Platform for the Detection of *Staphylococcus aureus*. *Analyst* **2020**, *145*, 4606−4614.
(36) Zhang, H.; Ma, X. Y.; Liu, Y.; Duan, N.; Wu, S. J.; Wang, Z. P.; Xu, B. C. Gold Nanoparticles Enhanced SERS Aptasensor for the Simultaneous Detection of *Salmonella typhimurium* and *Staphylococcus aureus*. *Biosens. Bioelectron.* **2015**, *74*, 872−877.
(37) Riu, J.; Giussani, B. Electrochemical Biosensors for the Detection of Pathogenic Bacteria in Food. *TrAC, Trends Anal. Chem.* **2020**, *126*, 115863.
(38) Rubab, M.; Shahbaz, H. M.; Olaimat, A. N.; Oh, D. H. Biosensors for Rapid and Sensitive Detection of *Staphylococcus aureus* in Food. *Biosens. Bioelectron.* **2018**, *105*, 49−57.
(39) Cao, X.; Li, S.; Chen, L.; Ding, H.; Xu, H.; Huang, Y.; Li, J.; Liu, N.; Cao, W.; Zhu, Y.; Shen, B.; Shao, N. Combining Use of a Panel Of ssDNA Aptamers in the Detection of *Staphylococcus aureus*. *Nucleic Acids Res.* **2009**, *37*, 4621−4628.
(40) Da, H.; Liu, H.; Zheng, Y.; Yuan, R.; Chai, Y. A Highly Sensitive VEGF165 Photoelectrochemical Biosensor Fabricated by Assembly of Aptamer Bridged DNA Networks. *Biosens. Bioelectron.* **2018**, *101*, 213−218.
(41) Xiao, Q.; Li, J.; Jin, X.; Liu, Y.; Huang, S. Ultrasensitive Electrochemical MicroRNA-21 Biosensor Coupling with Carboxylate-Reduced Graphene Oxide-Based Signal-Enhancing and Duplex-Specific Nuclease-Assisted Target Recycling. *Sens. Actuators, B* **2019**, *297*, 126740.
(42) Jia, F.; Duan, N.; Wu, S.; Ma, X.; Xia, Y.; Wang, Z.; Wei, X. Impedimetric Aptasensor for *Staphylococcus aureus* Based on Nanocomposite Prepared from Reduced Graphene Oxide and Gold Nanoparticles. *Microchim. Acta* **2014**, *181*, 967−974.
(43) Lee, C. W.; Chang, H. Y.; Wu, J. K.; Tseng, F. G. Ultra-Sensitive Electrochemical Detection of Bacteremia Enabled by Redox-Active Gold Nanoparticles (raGNPs) in a Nano-Sieving Microfluidic System (NS-MFS). *Biosens. Bioelectron.* **2019**, *133*, 215−222.
(44) Reich, P.; Stoltenburg, R.; Strehlitz, B.; Frense, D.; Beckmann, D. Development of an Impedimetric Aptasensor for the Detection of *Staphylococcus aureus*. *Int. J. Mol. Sci.* **2017**, *18*, 2484.
(45) Sun, Y.; He, X.; Ji, J.; Jia, M.; Wang, Z.; Sun, X. A Highly Selective and Sensitive Electrochemical CS-MWCNTs/Au-NPs Composite DNA Biosensor for *Staphylococcus aureus* Gene Sequence Detection. *Talanta* **2015**, *141*, 300−306.
(46) Abbaspour, A.; Norouz-Sarvestani, F.; Noori, A.; Soltani, N. Aptamer-Conjugated Silver Nanoparticles for Electrochemical Dual-Aptamer-Based Sandwich Detection of *Staphylococcus aureus*. *Biosens. Bioelectron.* **2015**, *68*, 149−155.

https://dx.doi.org/10.1021/acsami.0c22062
ACS Appl. Mater. Interfaces 2021, 13, 4905−4914